This document was prepared for the ETI by third parties under contract to the ETI. The ETI is making these documents and data available to the public to inform the debate on low carbon energy innovation and deployment.

Programme Area: Marine

Project: PerAWAT

Title: Validation and Verification of the Specwec Numerical Modeling Tool

Abstract:

This document describes the validation and verification of the SpecWEC numerical modeling tool with a linear hydrodynamic model (WAMIT), a non-linear hydrodynamic model (OXPOT), and wave tank experimental data from WG2 WP2. The document begins with a description of the method that is used to represent wave energy devices within the model. For this particular set of cases, a heaving buoy point absorber representation was developed. The specifics of the test cases are described. Twelve sea states with varying significant wave height, energy period, and directional characteristics were used for each configuration. A comparison of the SpecWEC tool to the wave tank experimental data from the Portaferry wave tank experiments is also presented. Finally, applications and limitations of the SpecWEC model are discussed.

Context:

The Performance Assessment of Wave and Tidal Array Systems (PerAWaT) project, launched in October 2009 with £8m of ETI investment. The project delivered validated, commercial software tools capable of significantly reducing the levels of uncertainty associated with predicting the energy yield of major wave and tidal stream energy arrays. It also produced information that will help reduce commercial risk of future large scale wave and tidal array developments.

Validation and Verification of the SpecWEC numerical modeling tool

WG1 WP2 D4 and D5

DOCUMENT CONTROL SHEET

Client	Energy Technologies Institute
Contact	Geraldine Newton-Cross
Project Title	PerAWaT
Document N^{o}	QUB-130131
Classification	Not to be disclosed except in line with the terms of the Technology Contract
Date	25th February 2013

REV.	Issue date	Purpose of issues	Prepared by	Checked by
1.0	31/01/13	Internal draft	KS	MF
2.0	31/01/13	Final draft for GH	KS	MF
3.0	26/02/13	Revised	KS	MF

Approved for release by: Matt Folley

CONTENTS

EXECUTIVE SUMMARY

This document contains deliverables WG1 WP2 D4 and D5, which contain the validation and verification of the SpecWEC numerical modeling tool with a linear hydrodynamic model (WAMIT), a non-linear hydrodynamic model (OXPOT), and wave tank experimental data from WG2 WP2. The document begins with a description of the method that is used to represent wave energy devices within the TOMAWAC spectral wave model. For this particular set of cases, a heaving buoy point absorber representation was developed. For each buoy at each time step, the amplitude of the incoming wave is determined from the spectral wave model, and then the dynamics of the device is solved using a frequency domain approach. Next, the power absorbed and the power radiated are calculated, which are finally converted into a change in the wave energy spectrum that is applied in the spectral wave equation.

Next, the specifics of the test cases are described. For both the model and wave tank comparison, the domain of the SpecWEC model was a rectangle with dimensions that were based on scaling up the wave tank experimental area to full scale. The parameters of the heaving buoy device in SpecWEC were based on a full scale version of the heaving buoy used in the wave tank testing. A linear power take off coefficient was used for simplicity in the linear and non-linear model comparisons, while a quasi-linear power take off coefficient was used in the wave tank comparison to be as accurate as possible. Isolated buoys were tested for the numerical models and wave tank data, and then four array layouts consisting of 4, 22, 24, and 24 devices respectively were also tested. Twelve sea states with varying significant wave height, energy period, and directional characteristics were used for each configuration.

WG1 WP2 D4 is presented next, which contains the comparison of the SpecWEC tool to the WAMIT linear potential flow model and the OXPOT non-linear potential flow model. Results are presented for all twelve sea states for isolated buoys and the total array power capture for each of the four configurations. The results from the numerical models and SpecWEC for the isolated buoys agree very well, whilst the difference between WAMIT and SpecWEC for the average power captures of the arrays is at most 23%. The q-factor (interaction factor) is also presented, and shows a general underestimate by the SpecWEC model. The results are then shown as a function of certain sea state parameters. It is demonstrated that the comparison between WAMIT and SpecWEC is best in sea states with smaller significant wave heights and worse when the energy period is larger. Finally, spatial error analysis of the array layouts indicates that larger differences between SpecWEC and WAMIT occur mostly in the middle of the arrays. Comparison of SpecWEC with the OXPOT numerical model for one sea state in the square configuration shows agreement in the power capture values of better than 15%.

WG1 WP2 D5 is presented next, which contains the comparison of the SpecWEC tool to the wave tank experimental data from the Portaferry wave tank experiments. The results presented are in a format identical to the results section in D4. The comparison between isolated buoys for the wave tank and SpecWEC is better than 16%, but the total array power capture shows larger differences of up to 60%. The q-factor tends to be overestimated by SpecWEC when compared to the wave tank data. When examining the results as a function of sea state parameters, it is seen that the best comparison occurs in directionally spread waves with a larger significant wave height and a large energy period.

Finally, applications and limitations of the SpecWEC model are discussed. Because of the phase-averaging nature of the spectral wave model, SpecWEC is incapable of resolving phase-dependent processes such as radiation and diffraction. This is evident in the buoy to buoy comparison of the SpecWEC model with the WAMIT model. It is therefore expected that SpecWEC will give better results when averaged over sea states and array layouts, which is demonstrated to be true. Investigation is ongoing into numerical methods for including more realistic radiation and diffraction representations in the SpecWEC model, which is expected to improve the estimate of the array interactions. The method for conversion of the power absorption for a device to a wave energy change is also discussed as a limitation of the model. It results in a time consuming calibration, so work is being done in an attempt to expedite that process.

1. INTRODUCTION

1.1. SCOPE OF DOCUMENT

The purpose of this document is to describe the comparison of the SpecWEC numerical modeling tool with a linear hydrodynamic model, a nonlinear hydrodynamic model, and wave tank experimental data. The SpecWEC numerical modeling tool is designed to assist in wave farm development by providing both an estimate of the power capture for each device in a wave farm and the effect of the presence of the wave farm on the incident ocean waves. The SpecWEC tool is a modification of an existing ocean spectral wave model, TOMAWAC. The modification of the TOMAWAC model to include a representation of wave energy devices is described in Section 4. First, the general theory for representing any type of wave energy device is included in Section 4.1. Then, the process for representing a heaving point absorber (as is used throughout this paper) is included in Section 4.2. Section 4.3 explains the applied method for converting the power absorbed by the heaving buoys into a change in the wave spectra. Finally, Section 4.4 describes the experimental setup for all of the comparison experiments.

Section 5 contains D4, which is the deliverable describing comparison of SpecWEC to a linear and a non-linear hydrodynamic model. The linear model used is the WAMIT potential flow model and the non-linear model is the OXPOT potential flow model. The results of comparison for each array configuration are presented individually for the linear model (Section 5.2) and the non-linear model (Section 5.3). Section 6 contains D5, which is the comparison of SpecWEC to the wave tank experimental data from WG2 WP2. Finally, in Section 7, the applications and limitations of SpecWEC are evaluated based on the comparison results.

1.2. RELATION TO OTHER DELIVERABLES

This report contains deliverables 4 and 5 from WG1 WP2. They describe the validation and verification of the SpecWEC numerical modeling tool. The representation of WECs used in SpecWEC was described in WG1 WP2 D1, and the implementation was described in WG1 WP2 D2. The beta software release of SpecWEC was WG1 WP2 D3. This report contains comparison with the wave tank data from WG2 WP2 D5.

1.3. ACCEPTANCE CRITERIA

The acceptance criteria for these deliverables are as follows:

1. Report contains details of model validation for a representative wave farm configuration and set of incident sea-states for point absorbers (and any other FDC if data available).
2. Report highlights applications and limitations of model and areas for improving the model.

Acceptance criterion 1 is fulfilled with the content in Sections 5 and 6, where the comparison of SpecWEC with the linear model, non-linear model, and wave tank experimental data for a heaving buoy-type wave energy converter are described; suitable models of another FDC are not currently available. Acceptance criterion 2 is fulfilled with the content in Section 7, where the applications and limitations of the model are discussed.

2. SPECWEC METHODS

2.1. GENERAL DESCRIPTION OF SPECWEC

The SpecWEC (Spectral representation of a Wave Energy Converter) numerical modelling tool is a modification of the TOMAWAC (TELEMAC-based Operational Model Addressing Wave Action Computation) spectral wave model. TOMAWAC, which was developed at EDF, like all third generation wave models solves

for the propagation of ocean surface wave energy through a domain. This is achieved by solving the wave action conservation equation, as follows:

$$\frac{\partial N}{\partial t} + \underbrace{\nabla_x \cdot \left[\left(\overrightarrow{c_g} + \vec{U}\right)N\right] + \frac{\partial c_\sigma N}{\partial \sigma} + \frac{\partial c_\theta N}{\partial \theta}}_{Convection\ terms} = \underbrace{\frac{S}{\sigma}}_{\substack{Source \\ terms}} \quad (1)$$

The left hand side of the conservation equation represents the changes in the ocean wave spectrum as it propagates through space. The source terms of the right hand side are parameterizations of mechanisms that add or remove energy from the ocean waves. Currently, the source term is typically broken down into six independent components, as follows:

$$S = S_{in} + S_{nl3} + S_{nl4} + S_{wc} + S_{db} + S_{bf} \quad (2)$$

where S_{in} represents generation of waves by the wind, S_{nl3} represents nonlinear triad interactions, S_{nl4} represents nonlinear quadruplet interactions, S_{wc} represents energy dissipation due to whitecapping, S_{db} depth-induced wave breaking, and finally S_{bf} represents bottom friction dissipation. These processes are all represented in a parameterized way; that is the process is not modeled explicitly in TOMAWAC, but the effect of these mechanisms is estimated and included as a source or sink of energy.

The representation of a wave energy converter in TOMAWAC is also achieved using a parameterized method. A new source term is incorporated into the right hand side of equation 1, so that the source term can now be broken down into 7 components:

$$S = S_{in} + S_{nl3} + S_{nl4} + S_{wc} + S_{db} + S_{bf} + S_{WEC} \quad (3)$$

There are two steps that are required in order to determine the source term strength for the WECs. First, the incoming wave field is used to calculate the power absorbed and radiated for each WEC device (Section 4.2). Next, the power absorbed is converted into a source term strength (Section 4.3).

2.2. CALCULATION OF ABSORBED AND RADIATED POWER

The SpecWEC tool is designed to enable a flexible representation of wave energy converters. For the numerical model comparison (D4) and the tank experimental data comparison (D5) presented here, a full scale heaving buoy wave energy device design was used. For each WEC in the domain, the power absorbed must be calculated at each time step. There are four steps to this calculation. First, the frequency-dependent wave component amplitudes are calculated from the spectral energy density. Next, the vertical displacement of each device associated with each wave component is calculated. The power absorbed is then calculated. Finally, the power radiated is calculated. These four steps are described in detail in the next four subsections.

2.2.1. CALCULATION OF WAVE AMPLITUDE

First, the incident wave amplitude as a function of frequency and direction must be calculated. The underlying assumption made by the TOMAWAC model is that a sea state can be represented as the linear superposition of plane progressive waves which have a random phase distribution:

$$\eta(x,t) = \sum_j a_j \cos\left(k_j x - \omega_j t + \varepsilon_j\right) \quad (4)$$

Here, a_j is the amplitude of the jth wave component, k is the wavenumber, ω is the angular wave frequency, and ε is the randomly distributed phase. Using this assumption of linearity, the energy present in a particular sea state can be expressed solely in terms of the wave component amplitudes as:

$$E(\omega,\theta) = \sum_{\omega}^{\omega+d\omega} \sum_{\theta}^{\theta+d\theta} \frac{1}{2}\rho g a_j^2 \qquad (5)$$

Therefore, given the directional spectrum of wave energy, it is possible to determine the free surface elevation in the following manner:

$$\eta(x,t) = \int_{\omega=0}^{\infty} \int_{\theta=0}^{2\pi} \sqrt{\frac{2}{\rho g} E(\omega,\theta)} \cos(kx - \omega t + \varepsilon)\, d\omega d\theta \qquad (6)$$

The individual wave component amplitudes can be solved for as:

$$a_j = \sqrt{\frac{2}{\rho g} E(\omega,\theta) d\omega d\theta} \qquad (7)$$

This information from TOMAWAC can then be used to calculate the vertical displacement of the heaving point absorber associated with each wave component.

2.2.2. CALCULATION OF RESPONSE

In order to solve for the motion of the WEC, several assumptions are made about the wave climate and the body motion. First, we assume that the wave steepness is small. It is also assumed that the WEC body motion has a small amplitude. And, as in the TOMAWAC model, it is assumed that the seastate may be represented as the linear superposition of plane progressive waves in which the phases are randomly distributed. For the following derivation, it is assumed that the WEC is a point absorber which only moves in the heave direction; however, it is straightforward to extend the following analysis to a device which has more than one degree of freedom.

From linearity, it follows that the WEC body displacement (in heave) $X(x,t)$ can be written in the form:

$$X(x,t) = Re\left(\sum_j I(\omega_j)\, e^{ik_j x - \omega_j t + \varepsilon_j} \right) \qquad (8)$$

where I is the frequency dependent complex response amplitude of the WEC. To progress we need to derive equations to solve for this particular quantity.

The WEC body equation of motion begins with the simple force acceleration balance which is outlined in Newton's second law: $F = ma$. Following the linearity assumptions described above, the forces on the WEC are represented in a linear fashion as follows:

$$F = A\frac{d^2X}{dt^2} + B\frac{dX}{dt} + \Lambda\frac{dX}{dt} + CX - D = M\frac{d^2X}{dt^2} \qquad (9)$$

where M is the mass of the body, A is an added mass coefficient representing the additional inertia due to the acceleration of the body in water, B is a damping coefficient corresponding to the energy radiated from the body into the water as waves, Λ is a damping coefficient corresponding to the power takeoff system of the WEC, and C is the system stiffness due to hydrostatic restoring forces. D represents wave exciting forces on the WEC body. Gathering like terms, this can be rewritten as:

$$D = (M + A)\frac{d^2X}{dt^2} + (B + \Lambda)\frac{dX}{dt} + CX \qquad (10)$$

Assuming that the exciting force D can also be written as the sum of individual frequency components $D = Re\left(\sum_j K(\omega_j) e^{i\omega_j}\right)$, this equation can be written in the frequency domain as:

$$I(\omega)\left(-\omega^2\left(M + A(\omega)\right) + i\omega(B(\omega) + \Lambda) + C\right) = K(\omega) \qquad (11)$$

The WEC body displacement is then solved for in terms of the added mass (A), radiation (B), power takeoff and loss(Λ), hydrostatic (C) and exciting force coefficients (k), and wave amplitude (a) as:

$$\boldsymbol{I(\omega) = \frac{k(\omega)a}{-\omega^2\big(M + A(\omega)\big) + i\omega(B(\omega) + \Lambda) + C}} \qquad (12)$$

2.2.3. CALCULATION OF POWER ABSORBED

Once the WEC displacement has been solved for, the energy absorbed by each WEC can be calculated. The energy absorption due to the power takeoff of the system is represented as follows:

$$\boldsymbol{P_{abs}(\omega) = \frac{1}{2} F_{PTO} \omega^2 |I(\omega)|^2} \qquad (13)$$

where $\boldsymbol{F_{PTO}}$ **is the power takeoff.** The power absorbed is introduced as a sink of energy in the wave action conservation equation at each time step.

2.2.4. CALCULATION OF POWER RADIATED

The power radiated as a function of frequency and direction is removed from the incoming wave spectrum at each WEC location. Because the heaving buoy is axi-symmetric then this power is reradiated equally in all directions as follows:

$$\boldsymbol{P_{rerad}(\omega) = \frac{\sum_\theta \frac{1}{2} \mathrm{B}(\omega) \omega^2 |I(\omega)|^2}{n_\theta}} \qquad (14)$$

Here $\boldsymbol{n_\theta}$ is the number of computational directions being used by TOMAWAC.

Because the radiation process conserves energy, the power that is radiated must be removed from the incident wave, as follows.[1] $\boldsymbol{P_{abs\_rad}(\omega) = \frac{1}{2} \mathrm{B}(\omega) \omega^2 |I(\omega)|^2}$ (15)

2.3. SOURCE TERM STRENGTH DETERMINATION

The power absorbed, radiated, and reradiated variables derived in the previous sections have units of Watts. However, the desired quantity for the source term strength is $\frac{W}{m^2}$ (power per area), because TOMAWAC solves for wave energy density, or wave energy per unit area. Therefore, in order to convert the power absorbed by the device into a source term strength to be fed into the TOMAWAC model, the area over which the power is absorbed must be designated. The method for converting the calculated power values into a source term strength for the TOMAWAC model involves the direct calculation of the area over which the power is absorbed. In this method, the source term strength is given as follows: $\boldsymbol{S_{WEC} = -\frac{P_{abs}}{A} - \frac{P_{rad}}{A} + \frac{P_{rerad}}{A}}$, where A is the area that must be designated. This area is determined using an iterative approach. The correct area can be determined by applying the divergence theorem, which states:

$$\boldsymbol{\iint_A \nabla \cdot \overrightarrow{Ec_g} dA = \oint \overrightarrow{Ec_g} \cdot \vec{n} dl = P_{abs}} \qquad (16)$$

where E is the wave energy spectral density and c_g is the wave group speed. That is, a path integral of the wave energy flux should equal the power absorbed by the device, as long as the integration path is closed and contains the wave energy device. If the conversion from the power absorbed to the source term strength applied in the TOMAWAC model is correct, then the two quantities will be the same. A set power absorption value was used, and the divergence theorem calculation was performed for each WEC location individually

[1] For axi-symmetric wave radiation the distribution of the radiated wave power is simple; however, for more complex modes the Kochin Function can be used to determine the distribution of radiated wave power. It may be expected, based on a super-position model of the incident and radiated waves that the modelling of the radiated wave is more complex. However, it can be shown that in the phase-averaged far-field then the effect of the radiated wave is to reduce the incident wave power by the sum of the absorbed/lost power and the radiated power, together with the radiation of wave power

using a rectangular integration path with approximately 150 metre sides. In this way, an area was designated for each WEC location used in the SpecWEC runs presented below.

2.4. MODEL RUN DETAILS

2.4.1. DOMAIN AND CONFIGURATION DETAILS

For all of the model runs described in the following sections (that is both for D4 and D5), the domain was chosen to mimic the physical wave tank testing in WG2 WP2 D5, but scaled up to full scale. The domain is a rectangle that spans 960 meters in the x direction and 360 meters in the y direction. The principle direction of wave propagation is along the positive y-axis, and the required directional wave spectra imposed on all 4 boundaries and initially throughout the domain. The domain had a constant water depth of 50 meters. The model was run with 30 directions and 26 computational frequencies. The computational meshes used for the various array configurations had a horizontal resolution of about 10 meters. Sensitivity studies on the mesh, directional, and frequency resolution were carried out and demonstrated that doubling any of these resolutions did not change the power capture results by more than 5%. Each model run had a time step of 0.5 seconds and lasted for 350 time steps, which was sufficient time to achieve a steady state in the domain. All the other spectral wave model source terms (such as whitecapping, bottom friction dissipation, etc.) besides the WEC source term were turned off.

2.4.2. HEAVING BUOY POINT ABSORBER

The WEC device used for the purposes of verification and validation of the SpecWEC numerical model is a heaving point absorber. The full scale heaving buoy is represented as a hemispherically-ended cylinder with a radius of 10 meters and a draft of 20 meters. The added mass, radiation, hydrostatic and exciting force coefficients used for the following wave tank and numerical model comparisons were obtained using the WAMIT potential flow model. Two different power takeoff representations were used. For the numerical model comparison (D4), a linear power takeoff coefficient representation with a value of 7×10^6 kg/s was applied, in order to simplify the comparison as much as possible.

For the physical wave tank data comparison (D5), a nonlinear Coulomb friction damping representation was used, in order to mimic the actual heaving buoy model. The power takeoff and power loss were calculated separately:

$$\boldsymbol{\Lambda = F_{PTO} + F_{loss}} \qquad (17)$$

$$\boldsymbol{F_{PTO} = \sqrt{\frac{2}{\pi}}\ \frac{D}{\hat{v}}} \qquad (18)$$

$$\boldsymbol{F_{loss} = B_l + 2B_v\sqrt{\frac{2}{\pi}}\hat{v}} \qquad (19)$$

Here, D is the Coulomb friction damping coefficient, B_l is the linear loss coefficient, $B_v$is the quadratic loss coefficient, and $\hat{v}$ is the expected velocity, calculated as follows:

$$\boldsymbol{\hat{v} = \sum_{i=1}^{i=N} \frac{1}{2}\omega_i^2 |I_i|^2} \qquad (19)$$

The Coulomb friction damping coefficient used was 204.8 kN, in accordance with the value used for the tank (0.4 N at 80^{th} scale). Additional linear and quadratic damping terms were also included in the SpecWEC model for the tank comparison in order to represent losses of the heaving buoy models. Possible sources of these losses include the bearing mechanism, skin friction and vortex shedding. These damping

terms were not included in the calculation of the absorbed power and therefore are not considered to be part of the power take off system. The coefficients of the linear and quadratic damping terms were calibrated using the isolated buoy power capture values by minimizing the average error between the power capture of the wave tank model and that calculated by SpecWEC. The linear damping coefficient used was 2.5×10^5 Ns/m and the quadratic damping coefficient was 6.4×10^4 Ns^2/m^2.

2.4.3. WEC LAYOUTS

First, an isolated buoy run was carried out for each sea state. Then, model runs were carried out for each of the four WEC array configurations that were used for the physical tank testing: Square, Configuration A, Configuration B, and Configuration C (Figure 1). Configuration A was designed as a standard staggered row layout, while configurations B and C were designed using an optimization technique to achieve maximum power capture and minimum power capture respectively.

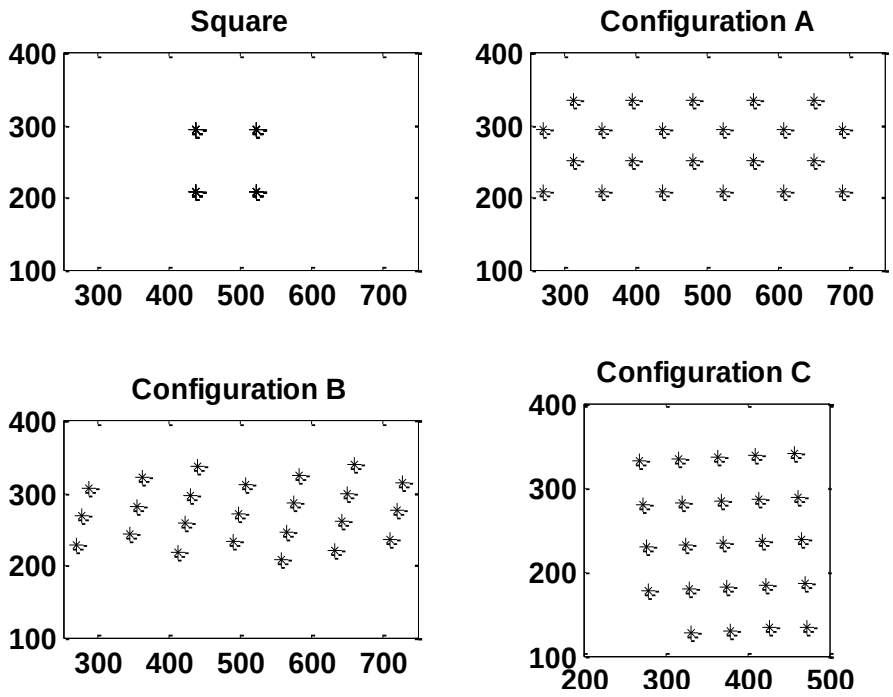

FIGURE 1: FOUR CONFIGURATIONS USED FOR THE MODEL VERIFICATION AND VALIDATION.

2.4.4. SEA STATES

Because SpecWEC is a spectral wave model, it is not capable of accurately representing monochromatic sea states. Therefore, all comparisons used only the polychromatic sea states defined for the wave tank testing. This consisted of 12 polychromatic sea states with varying energy period, significant wave height, directional spreading, steepness, and mean wave direction, as shown in Table 1. Because spectral wave models cannot simulate unidirectional seas directly, a sea with very little spreading, i.e. s=45, was used as an approximation.

Sea-state	H_s	T_e	γ	s	PWD	Steepness
01	2.0	6.5	2.0	45	0	0.03
02	2.0	8.0	1.0	45	0	0.02
03	2.0	11.3	1.0	45	0	0.01
04	3.0	11.3	1.0	45	0	0.02
05	2.0	8.0	1.0	15	0	0.02
06	3.0	11.3	1.0	15	0	0.02
07	2.0	8.0	1.0	3	0	0.02
08	3.0	11.3	1.0	3	0	0.02
09	2.0	8.0	1.0	45	15	0.02
10	3.0	11.3	1.0	45	15	0.02
11	2.0	8.0	1.0	45	25	0.02
12	3.0	11.3	1.0	45	25	0.02

TABLE 1: SEA STATE PARAMETERS

3. D4: COMPARISON WITH LINEAR AND NONLINEAR NUMERICAL MODELS

3.1. WAMIT MODEL RUNS

In order to achieve the comparison of the SpecWEC tool with a linear numerical model, the linear potential flow model WAMIT was used. The WAMIT model was run with 81 computation frequencies and 2 degree directional resolution for all four WEC configurations as well as for an isolated buoy. As mentioned previously, a linear damping coefficient was used to represent the power takeoff coefficient on the heaving buoy. The results from the comparison for isolated buoys as well as all four configurations are presented below.

3.2. WAMIT COMPARISON RESULTS

Power capture results for both the WAMIT model runs and the SpecWEC model runs are shown below (Section 5.2.1 to Section. 5.2.5). First, the results for the isolated buoy are shown for all 12 sea states. Next, the total power capture for each of the four arrays (Square, Configuration A, Configuration B, and Configuration C) for both WAMIT and SpecWEC is compared for each sea state. The q-factor (interaction factor) is then displayed as a function of sea state. The total array power capture results are next broken down by comparing results from sea states with varying directional spreading and angled waves, varying significant wave height, and varying peak period. Finally, the spatial distribution of the errors averaged over the sea states within the arrays is shown.

3.2.1. COMPARISON WITH ISOLATED BUOY

Comparison of the power capture of an isolated buoy for both WAMIT and SpecWEC show good agreement for all twelve sea states, Table 2. Because WAMIT and SpecWEC use the same equations for calculation of the WEC displacement and power absorbed, this result confirms the correct implementation of those equations in the SpecWEC model.

Sea-state	WAMIT power capture (kW)	SpecWEC power capture (kW)
01	10.5	10.6
02	29.4	29.5
03	71.1	71.3
04	160.1	160.5
05	29.4	29.5
06	160.1	160.5
07	29.4	29.4
08	160.1	160.1
09	29.4	29.5
10	160.1	160.5
11	29.4	29.5
12	160.1	160.5

TABLE 2: ISOLATED BUOY POWER CAPTURE FOR WAMIT AND SPECWEC

3.2.2. ARRAY POWER CAPTURE

	Square			Configuration A			Configuration B			Configuration C		
	WAMIT	SpecWEC	% Error	WAMIT	SpecWEC	% Error	WAMIT	SpecWEC	% Error	WAMIT	SpecWEC	% Error
SS1	40.6	40.8	1	216.8	224.2	3	218.6	231.3	6	260.7	221.4	15
SS2	117.9	111.3	6	604.5	610.4	1	719.8	606.4	16	650.1	568.4	13
SS3	281.9	265.7	6	1571.8	1456.0	7	1811.2	1415.1	22	1640.0	1314.8	20
SS4	634.2	597.9	6	3536.5	3276.1	7	4075.3	3183.9	22	3690.0	2958.4	20
SS5	115.9	113.1	2	606.1	611.2	1	706.6	626.2	11	643.6	566.6	12
SS6	630.4	610.4	3	3515.8	3282.3	7	4023.9	3314.3	18	3685.7	2946.3	20
SS7	113.7	114.1	0	577.3	590.6	2	660.2	624.2	5	621.8	568.0	9
SS8	626.4	617.0	2	3329.6	3147.1	5	3723.6	3302.4	11	3580.5	2953.1	18
SS9	116.0	113.2	2	606.0	614.2	1	694.1	617.0	11	639.4	589.2	8
SS10	630.4	610.6	3	3519.3	3302.4	6	4007.0	3253.9	19	3664.8	3092.2	16
SS11	113.2	115.2	2	610.3	612.7	0	678.7	642.6	5	629.2	589.1	6
SS12	625.1	624.4	0	3491.5	3293.7	6	3922.4	3422.6	13	3649.1	3090.0	15

TABLE 3: ARRAY POWER CAPTURE FOR WAMIT AND SPECWEC

The total array power captures calculated by WAMIT and SpecWEC show agreement with less than 10% for the square and Configuration A layouts, and agreement with less than 23% error for the Configuration B and Configuration C layouts. There is particularly good agreement in all layouts in Sea States 7 and 11, which have the smaller significant wave height and an energy period of 8 seconds. Sea states 5 and 9, which have the same significant wave height and energy period, also show better agreement than the sea states with larger significant wave height and energy period. There is an overall tendency for the SpecWEC total power capture to be smaller than the WAMIT total power capture, particularly in Configurations B and C.

3.2.3. Q-FACTOR

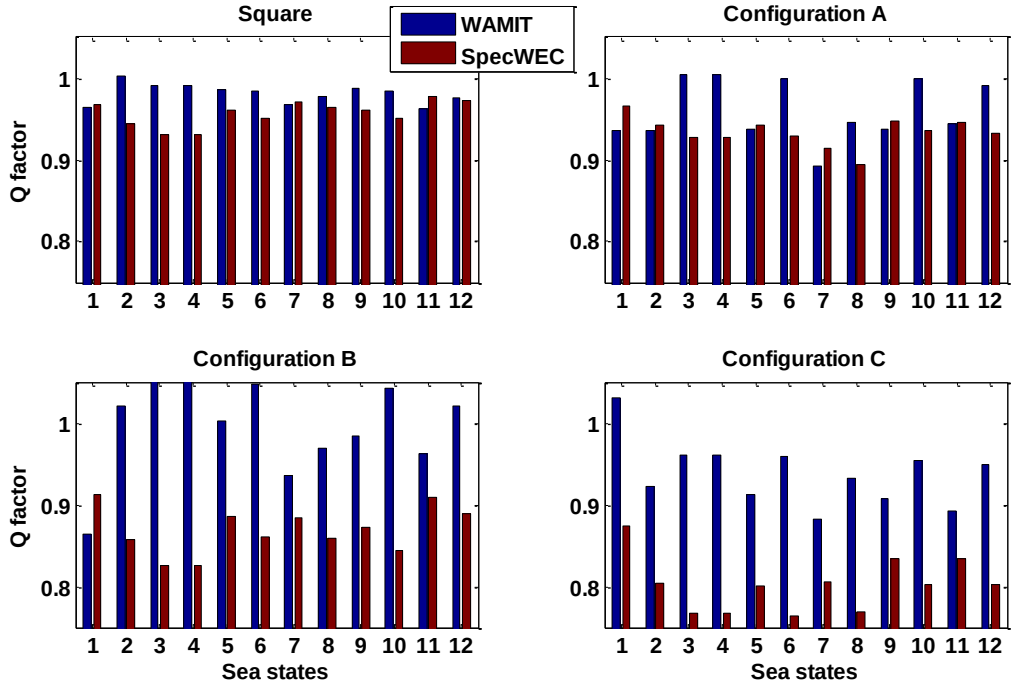

FIGURE 2: Q-FACTOR FOR WAMIT (BLUE) AND SPECWEC (RED) FOR ALL 4 ARRAY LAYOUTS

As in the total array power capture, there is a tendency for SpecWEC to underestimate the q-factor (i.e. over-estimate destructive array interactions or under-estimate constructive array interactions), particularly in Configurations B and C.

Square			Configuration A			Configuration B			Configuration C		
WAMIT	SpecWEC	%Error	WAMIT	SpecWEC	%Error	WAMIT	SpecWEC	%Error	WAMIT	SpecWEC	%Error
0.98	0.96	2	0.96	0.93	3	1.00	0.87	13	0.94	0.80	15

TABLE 4: Q-FACTOR AVERAGED OVER ALL 12 SEA STATES

To match the WAMIT predictions, the SpecWEC average q-factor should be smallest for Configuration C and largest for Configuration B. However, whilst the SpecWEC average q-factor is smallest for Configuration C, the largest q-factor occurs for Configuration A. It is suggested that this reflects inaccurate estimation of phase-dependent array interactions by SpecWEC.

3.2.4. SEA STATE PARAMETER DEPENDENCE

3.2.4.1. DIRECTIONAL DEPENDENCE

	Square			Configuration A			Configuration B			Configuration C		
	WAMIT	SpecWEC	% Error	WAMIT	SpecWEC	% Error	WAMIT	SpecWEC	% Error	WAMIT	SpecWEC	% Error
SS 1-4	1074.5	1015.8	5	5929.6	5566.8	6	6825.0	5436.7	20	6240.8	5063.0	19
SS 5-8	1486.4	1454.5	2	8028.8	7631.3	5	9114.3	7867.0	14	8531.6	7034.1	18
SS 9-12	1484.7	1463.4	1	8227.2	7823.0	5	9302.2	7936.0	15	8582.5	7360.6	14

TABLE 5: DIRECTIONAL DEPENDENCE OF THE TOTAL POWER CAPTURE FOR THE 4 ARRAY CONFIGURATIONS

This table was generated by summing the total power capture results over the sea states that have no directional spread and no angled waves (sea states 1-4), the sea states with directional spread and no angled waves (sea states 5-8), and the sea states with no directional spread but that include angled waves (sea states

9-12). It can be seen that the sea states with no directional spread and no angled waves give the worst comparison between SpecWEC and WAMIT, while SpecWEC performs best in angled waves except for in Configuration B.

3.2.4.2. SIGNIFICANT WAVE HEIGHT DEPENDENCE

	Square			Configuration A			Configuration B			Configuration C		
	WAMIT	SpecWEC	% Error	WAMIT	SpecWEC	% Error	WAMIT	SpecWEC	% Error	WAMIT	SpecWEC	% Error
Hs = 2	899.1	873.4	3	4792.9	4719.5	2	5489.2	4762.7	13	5084.8	4417.7	13
Hs = 3	3146.5	3060.2	3	17392.8	16301.6	6	19752.3	16477.1	17	18270.0	15039.9	18

TABLE 6: SIGNIFICANT WAVE HEIGHT DEPENDENCE OF TOTAL ARRAY POWER CAPTURE.

This table was generated by summing the total power capture results over those sea states that have significant wave height of 2 m, and those that have significant wave height of 3 m. In all of the array configurations (except the square) that SpecWEC and WAMIT agree more in sea states with significant wave height of 2 m. This may be due to phase-dependent array interactions (which are resolved by WAMIT and not SpecWEC) being more pronounced in larger sea states.

3.2.4.3. ENERGY PERIOD DEPENDENCE

	Square			Configuration A			Configuration B			Configuration C		
	WAMIT	SpecWEC	% Error	WAMIT	SpecWEC	% Error	WAMIT	SpecWEC	% Error	WAMIT	SpecWEC	% Error
Te = 6.5	40.6	40.8	1	216.8	224.2	3	218.6	231.3	6	260.7	221.4	15
Te = 8.0	576.6	566.9	2	3004.3	3039.2	1	3459.4	3116.3	10	3184.1	2881.4	10
Te = 11.3	3428.3	3326.0	3	18964.6	17757.7	6	21563.5	17892.2	17	19910.0	16354.8	18

TABLE 7: ENERGY PERIOD DEPENDENCE OF TOTAL ARRAY POWER CAPTURE

This table was generated by summing the total power capture results over sea states that have an energy period of 6.5 s, those that have an energy period of 8.0 s. and those that have an energy period of 11.3 s. The SpecWEC and WAMIT comparison is worst when the energy period is 11.3 seconds, and the best comparison depends on the array configuration.

3.2.5. SPATIAL ERROR DISTRIBUTION

In order to look at the spatial distribution of the differences between the WAMIT and SpecWEC results in each array, a percent difference normalized by the isolated buoy values was calculated as follows:

$$\boldsymbol{Err = 100 * \left| \frac{P_{array}}{P_{isolated_{WAMIT}}} - \frac{P_{array}}{P_{isolated_{SpecWEC}}} \right|} \quad (\mathbf{15})$$

This calculation was performed for each buoy in all of the array layouts, and then averaged over all 12 sea states. The resulting values are plotted for each configuration in Figure 3. For the square configuration, the differences between the two models are higher in the second row than in the first. For configurations A and B, the largest differences between the two models appear in the middle of the arrays. For configuration C, the largest differences between the two models span from the front of the array all the way to the back of the array, but are isolated to the right side of the array.

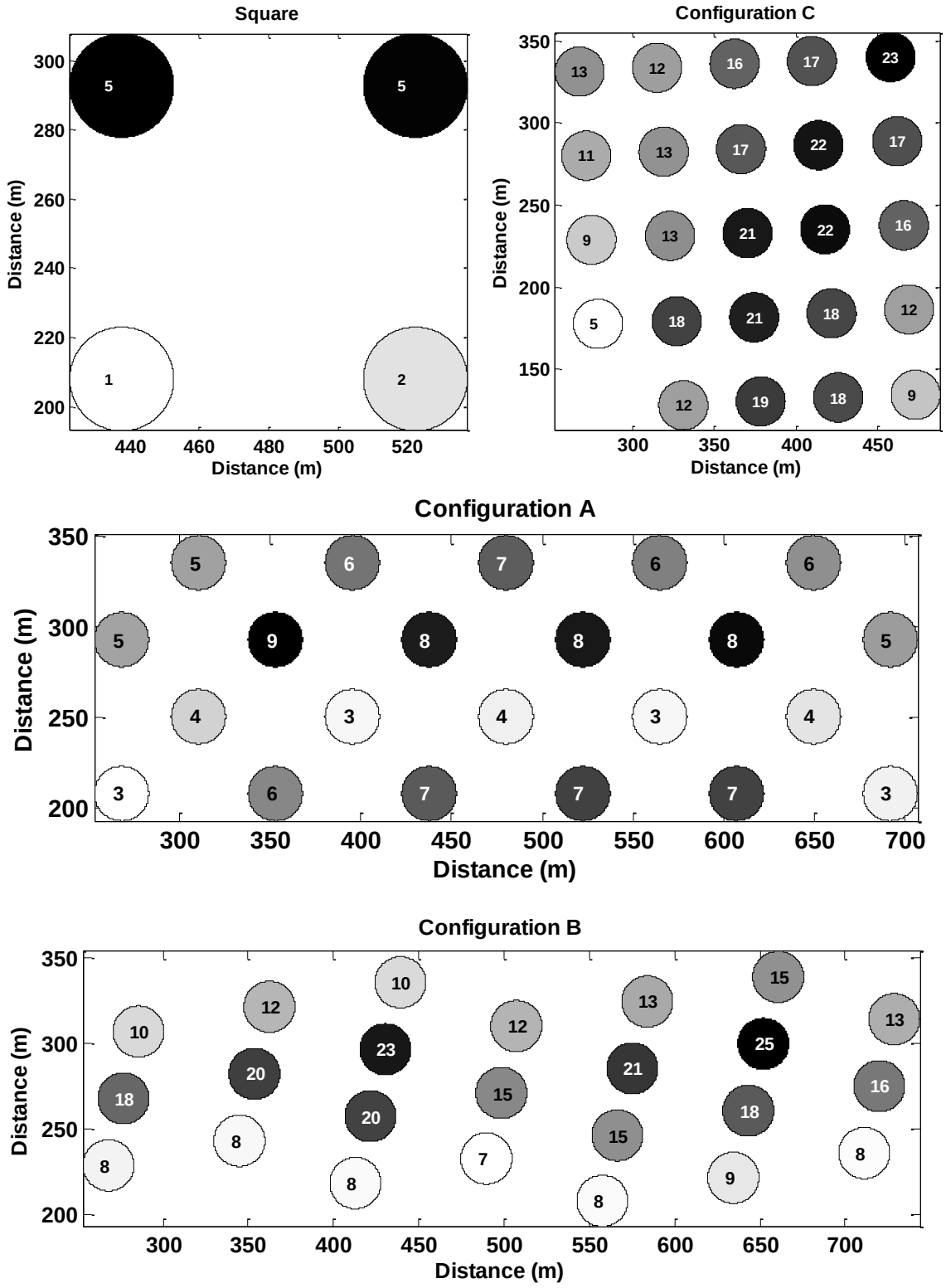

FIGURE 3: NORMALIZED PERCENT DIFFERENCE BETWEEN WAMIT AND SPECWEC FOR SQUARE CONFIGURATION (TOP LEFT), CONFIGURATION C (TOP RIGHT), CONFIGURATION A (MIDDLE) AND CONFIGURATION B (BOTTOM).

3.3. NON-LINEAR COMPARISON RESULTS

In order to achieve comparison with a non-linear potential flow model, the OXPOT model was run in the square configuration for sea state 3, using the same linear power take off coefficient that was used throughout D4. Because of the significant processing time required by OXPOT this is the only sea state modeled. The

results, presented below, show an agreement between the two models of better than 15%, with an underestimation of SpecWEC of the power capture values given by OXPOT. However, analysis of the OXPOT results for two different numerical tank widths suggested that the uncertainty for the given power capture values were at least 8.5 kW or approximately 12%. Given this fact, the power capture values for SpecWEC are within the error estimates for OXPOT for the front row of the square, and only just smaller than the error estimates for OXPOT for the second row of the square.

3.3.1. SQUARE COMPARISON

	Power capture (kW)				Sum Power Capture
OXPOT					
SS3	79.00	72.10	79.00	72.10	302.20
SpecWEC					
SS3	71.36	61.90	71.33	61.14	265.73
Percent error (%)					
SS3	10	14	10	15	12

TABLE 8: POWER CAPTURE RESULTS FOR SPECWEC AND OXPOT

4. D5: COMPARISON WITH WAVE TANK EXPERIMENTAL DATA

4.1. WAVE TANK DATA

The wave tank data presented here for comparison with the SpecWEC model is from the WG2 WP2 experiments carried out in Portaferry. These data were described in detail in the WG2 WP2 D5. Only the polychromatic data is used here.

4.2. RESULTS

4.2.1. COMPARISON WITH ISOLATED BUOY

Following model calibration, as described in section 4.4.2, the results for the isolated buoy comparison between SpecWEC and the wave tank power capture agree to better than 16%, as shown in Table 9.

Sea-state	Wave tank power capture (kW)	SpecWEC power capture (kW)
01	20.4	23.5
02	63.3	58.1
03	59.3	59.1
04	106.8	97.1
05	58.0	58.1
06	95.0	97.1
07	61.3	57.9
08	101.9	96.9
09	50.6	58.1
10	89.3	97.1
11	69.3	58.1
12	103.0	97.1

TABLE 9: ISOLATED BUOY POWER CAPTURE IN KW FOR SPECWEC AND THE WAVE TANK

4.2.2. ARRAY POWER CAPTURE

	Square			Configuration A			Configuration B			Configuration C		
	Tank	SpecWEC	% Error	Tank	SpecWEC	% Error	Tank	SpecWEC	% Error	Tank	SpecWEC	% Error
SS1	93.5	85.1	9	287.4	460.2	60	333.4	428.0	28	337.5	405.3	20
SS2	223.1	214.3	4	1049.9	1186.1	13	1394.4	1112.4	20	874.2	1082.7	24
SS3	220.5	222.7	1	1176.6	1213.2	3	1382.5	1192.6	14	1097.4	1165.1	6
SS4	375.7	369.0	2	1999.3	2027.6	1	2421.1	2016.1	17	1810.4	1987.7	10
SS5	217.0	218.5	1	1013.4	1181.2	17	1275.7	1165.9	9	924.0	1060.4	15
SS6	375.4	373.8	0	1777.3	2021.1	14	2141.6	2073.3	3	1740.6	1958.4	13
SS7	210.2	220.7	5	1050.7	1105.2	5	1306.4	1143.5	12	969.7	1038.0	7
SS8	391.1	375.9	4	1860.1	1929.9	4	2250.8	2042.8	9	1852.3	1924.9	4
SS9	202.4	219.6	8	926.0	1196.0	29	1129.8	1152.5	2	851.3	1145.0	34
SS10	348.1	375.0	8	1761.5	2038.1	16	2088.5	2059.1	1	1750.5	2059.2	18
SS11	228.8	224.7	2	1054.1	1194.0	13	1371.3	1229.5	10	968.8	1144.5	18
SS12	358.2	380.5	6	1757.1	2034.0	16	2204.2	2144.0	3	1845.5	2057.4	11

TABLE 10: ARRAY POWER CAPTURE FOR WAVE TANK AND SPECWEC

The total array power capture comparison between the wave tank and SpecWEC shows agreement of better than 10% in the square configuration, with agreements of better than 28% and 34% in configurations B and C respectively. There are large differences in the first sea state that are not unexpected as the waves were small and not near the resonant period, so that at times the buoy motion would stall. The current spectral model for coulomb friction assumes constant motion and thus is not capable of adequately modelling stall, which results in larger errors in this sea state.

4.2.3. Q-FACTOR

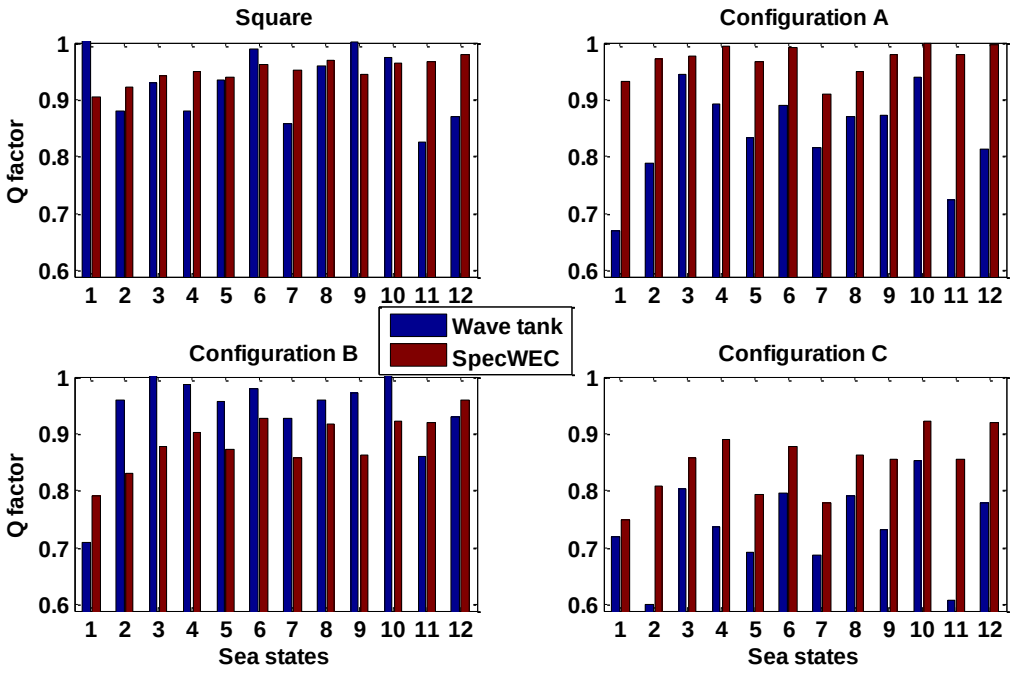

FIGURE 4: Q-FACTOR FOR WAVE TANK (BLUE) AND SPECWEC (RED) FOR ALL 4 ARRAY LAYOUTS

The wave tank q-factor is overestimated consistently by SpecWEC in Configurations A and C, but this is not true in configuration B or the square array layout.

Square			Configuration A			Configuration B			Configuration C		
Tank	SpecWEC	% Error	Tank	SpecWEC	% Error	Tank	SpecWEC	% Error	Tank	SpecWEC	% Error
0.94	0.95	1	0.84	0.97	16	0.94	0.89	6	0.73	0.85	16

TABLE 11: Q-FACTOR AVERAGED OVER ALL 12 SEA STATES

To match the wave tank data, the SpecWEC average q-factor should be smallest for Configuration C and largest for Configuration B. However, whilst the SpecWEC average q-factor is smallest for Configuration C, the largest q-factor occurs for Configuration A. It is suggested that this may reflect inaccurate estimation of phase-dependent array interactions by SpecWEC.

4.2.4. SEA STATE PARAMETER DEPENDENCE

The following tables were generated in a similar fashion to those tables in Section 5.2.4, that is by summing the total array power capture over various sea states depending on parameters including directional spread and angling, significant wave height, and energy period.

4.2.4.1. DIRECTIONAL DEPENDENCE

	Square			Configuration A			Configuration B			Configuration C		
	Tank	SpecWEC	% Error	Tank	SpecWEC	% Error	Tank	SpecWEC	% Error	Tank	SpecWEC	% Error
SS 1-4	912.8	891.2	2	4513.2	4887.1	8	5531.4	4749.1	14	4119.5	4640.8	13
SS 5-8	1193.7	1189.0	0	5701.5	6237.3	9	6974.4	6425.5	8	5486.5	5981.7	9
SS 9-12	1137.4	1199.7	5	5498.6	6462.2	18	6793.9	6585.1	3	5416.1	6406.2	18

TABLE 12: DIRECTIONAL DEPENDENCE OF THE TOTAL POWER CAPTURE FOR THE 4 ARRAY CONFIGURATIONS

The comparison between SpecWEC and the wave tank data shows the best agreement for sea states with directional spread and no angled waves in all of the configurations except for Configuration A. The worst comparison is found in the angled waves for all of the configurations except Configuration B.

4.2.4.2. SIGNIFICANT WAVE HEIGHT DEPENDENCE

	Square			Configuration A			Configuration B			Configuration C		
	Tank	SpecWEC	% Error	Tank	SpecWEC	% Error	Tank	SpecWEC	% Error	Tank	SpecWEC	% Error
Hs = 2	1395.4	1405.7	1	6558.0	7535.8	15	8193.5	7424.4	9	6022.9	7041.0	17
Hs = 3	1848.5	1874.2	1	9155.3	10050.7	10	11106.2	10335.4	7	8999.3	9987.7	11

TABLE 13: SIGNIFICANT WAVE HEIGHT DEPENDENCE OF TOTAL ARRAY POWER CAPTURE.

For all of the configurations, the comparison between SpecWEC and the tank data is the best in sea states with significant wave height of 3 m.

4.2.4.3. ENERGY PERIOD DEPENDENCE

	Square			Configuration A			Configuration B			Configuration C		
	Tank	SpecWEC	% Error	Tank	SpecWEC	% Error	Tank	SpecWEC	% Error	Tank	SpecWEC	% Error
Te = 6.5	93.5	85.1	9	287.4	460.2	60	333.4	428.0	28	337.5	405.3	20
Te = 8.0	1081.4	1097.8	2	5094.0	5862.4	15	6477.6	5803.8	10	4588.0	5470.6	19
Te = 11.3	2069.0	2096.9	1	10331.9	11263.9	9	12488.7	11527.9	8	10096.6	11152.8	10

TABLE 14: ENERGY PERIOD DEPENDENCE OF TOTAL ARRAY POWER CAPTURE.

The comparison between SpecWEC and the wave tank data is consistently worst for energy period of 6.5 s, and the best for sea states with energy period of 11.3 seconds.

4.2.5. SPATIAL ERROR DISTRIBUTION

The following figures contain the normalized percent difference between SpecWEC and the wave tank data, and were generated using the method described in Section 5.2.5. Because the wave tank data is experimental data (and therefore subject to inherent errors such as buoy differences and wave tank inhomogeneity), these percent difference results don't display as strong patterns as those in the model comparison. For example, in Configuration A, the results indicate that differences are larger near the back of the array, while in Configuration B the largest differences are found throughout the array.

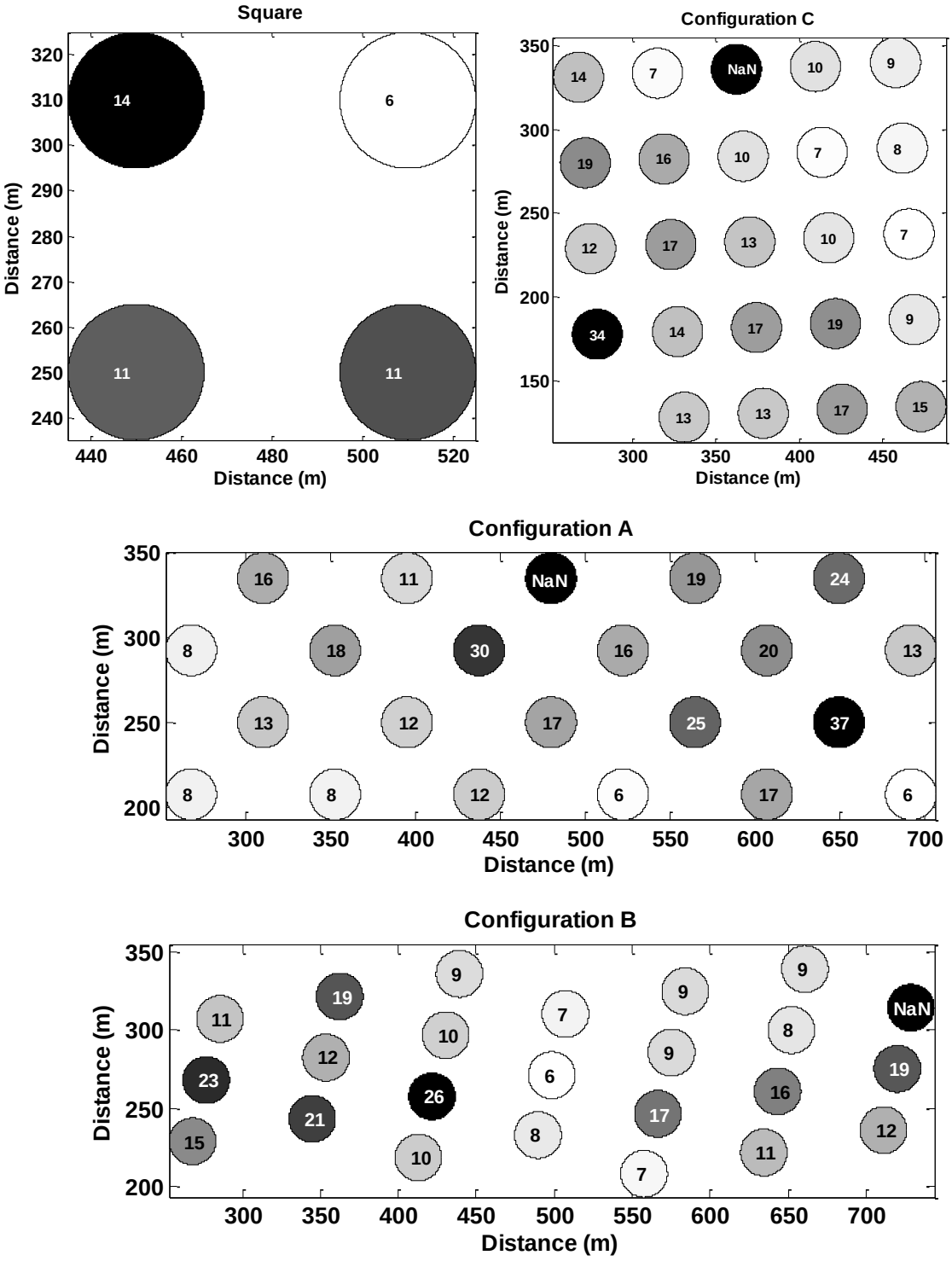

FIGURE 5: NORMALIZED PERCENT DIFFERENCE BETWEEN WAVE TANK AND SPECWEC FOR SQUARE CONFIGURATION (TOP LEFT), CONFIGURATION C (TOP RIGHT), CONFIGURATION A (MIDDLE) AND CONFIGURATION B (BOTTOM).

5. APPLICATIONS AND LIMITATIONS OF SPECWEC

The purpose of this comparison of the SpecWEC model to both other numerical models and wave tank experimental data is to determine the suitability of the SpecWEC model for use in power capture estimations for large WEC arrays. Because the SpecWEC model is based on a spectral wave model that is phase-averaged, it is incapable of representing close WEC array interactions that are phase-dependent. Therefore, it is not expected that the SpecWEC model can exactly reproduce the power capture of individual buoys in an array. However, it is hoped that the model will be able to provide useful information to the user about the total power production of an array. Averaging over all sea states and configurations, the agreement between total array power production calculated by SpecWEC and the WAMIT model is better than 9%, and the agreement between total array power production calculated by SpecWEC and the wave tank data is better than 12%. These small values indicate that SpecWEC can be a useful tool for power production estimation, particularly when averaging over a large number of devices and sea states. It should also be noted that there are inherent errors and assumptions associated with the wave tank data and the WAMIT model that have not been addressed here. The WAMIT model makes several assumptions, including linearity of the buoy motion, potential flow, and the linearity of the ocean waves. Likewise, there are errors inherent in the wave tank data, including individual buoy differences and the non-homogeneity of the waves in the wave tank at the device locations. These issues increase the uncertainty of both the wave tank and WAMIT model data, suggesting that the agreement between SpecWEC and these could potentially be clarified by placing error bars on the comparison data.

The current implementation of SpecWEC includes phase-averaged approximations of the energy absorbed and the energy radiated by the WEC. However, energy will also be re-distributed by diffraction from the WEC, which is currently not included within the SpecWEC model. The reason that diffraction is not currently included in the SpecWEC model is because there is not currently a suitable phase-averaged representation of diffraction due to a body that can be used. Notwithstanding this current limitation, recent developments in modelling WECs have indicated that it should be possible to use the far-field asymptotic approximation of Kochin Functions to produce a phase-averaged representation of WEC diffraction. It would be expected that when this phase-averaged representation of WEC diffraction is included in SpecWEC that the accuracy of the model will be improved.

One of the fundamental limitations of SpecWEC is the inability to represent phase-dependent processes, such as constructive and destructive interference due to radiation and diffraction of waves around devices, whilst it is argued that as the separation distance between WECs increases the constructive and destruction interference patterns at different frequencies tend to cancel each other out so that a phase-averaged approximation becomes reasonable. However, the array layouts modeled are relatively closely spaced and the significance of phase-dependent interactions is evident when comparing SpecWEC to the WAMIT model on an individual device basis. It can be seen in Figure 3 that the largest differences between SpecWEC and the WAMIT model are found in the centre of the array layouts, and this is probably due to the phase-dependent diffraction and radiation as calculated by WAMIT being more significant in the centre of the array. However, the idealized hydrodynamics as represented by WAMIT are not always fully representative of physical scenarios and may highlight issues that are not as significant as they may at first appear. This can be seen in the comparison of SpecWEC with the wave tank model results, which do not exhibit the same pattern of differences across the array and the largest differences are not focused in the middle of the arrays. Similarly, the performance of WECs in actual wave farms may also be affected by factors such as individual WEC variations, local marine currents, variations in water depth, etc. so that the apparent significance of phase-dependent interactions as predicted by linear potential flow models may be misleading.

Another current limitation of the SpecWEC model is the area method that is used to determine the source term strength from the power calculations. Although accurate, the calculation of the representative

area of every WEC location is time consuming for large arrays of devices. However, based on initial investigations, the calculation of the correct area simply from mesh parameters is not straightforward. It seems likely that this area is dependent on the method of characteristics that is used to solve for the propagation of the waves in TOMAWAC. Collaboration with the development team of TOMAWAC is being undertaken in an attempt to resolve this issue so that the representative area can be explicitly defined.

In conclusion, the comparison of SpecWEC with numerical and physical models has indicated that the SpecWEC concept is generally valid and can currently produce reasonable estimates of wave farm performance. However, the validation process has also highlighted a number of areas in which SpecWEC can be improved, both in the representative of the WECs (by inclusion of body diffraction) and in the implementation of the WEC source term in TOMAWAC. The validation process has indicated that SpecWEC may not capture all of the detailed hydrodynamic interactions when the WECs are close-packed, but that for actual wave farms this is not likely to be significant.

APPENDIX A: INTERACTION BETWEEN A WEC AND THE INCIDENT WAVE

It has been noted that Kochin functions may provide a method by which array interactions can be modelled efficiently. Kochin functions can be used to represent both the diffracted and radiated wave fields. For these to be used with a spectral wave model it is necessary that a phase-averaged representation exists. Here, expressions for far-field approximations of the radiated and diffracted waves are derived, which can then be related to the appropriate Kochin function. It is shown that in the far-field approximation, the change in the wave energy due to the presence of a WEC can be decomposed into the sum of a radiation and a power absorption term.

The analysis below essentially combines the incident and radiated/diffracted wave travelling at an angle ϑ. This is used to calculate expressions for the energy flux, which is decomposed into energy flux associated with the incident wave, the radiated/diffracted wave and the interaction between these two waves. The energy flux associated with the incident and radiated/diffracted waves is non-oscillatory and easy to calculate; however, the energy flux oscillates due to the interactions as the waves go in and out of phase.

This interaction term is analysed further and using the Reimann-Lebesgue Lemma and the Method of Stationary Phase it is possible to generate an expression for this component in the far-field. It is shown that in the far-field the only persistent effect is a change in the energy flux in the direction of incident wave propagation.

Finally the derived expressions for energy flux are used to calculate the maximum power capture of a monopole wave energy converter. It is found that calculation produces the correct result as has been derived elsewhere.

A.1 DERIVATION

$$\widetilde{U}_x = \left[1 + \left(\frac{i}{2kr} + 1\right)\frac{H(\theta)}{\sqrt{kr}}\cos\theta\, e^{i\phi(\theta)}\right]$$

$$\widetilde{U}_y = \left[\left(\frac{i}{2kr} + 1\right)\frac{H(\theta)}{\sqrt{kr}}\sin\theta\, e^{i\phi(\theta)}\right]$$

So now

$$\vec{U} = \Re\left(\left(\widetilde{U}_x\vec{x} + \widetilde{U}_y\vec{y}\right)\omega\eta_i e^{kz}e^{i(kx-\omega t)}\right)$$

The average wave energy flux is essentially unchanged as

$$\vec{j} = \frac{\rho g\omega\eta^2}{2k}\frac{1}{\mathrm{T}}\int_{\mathrm{t}}^{\mathrm{t+T}} \Re\left(\left(1 + \frac{H(\theta)}{\sqrt{kr}}e^{i\phi(\theta)}\right)e^{i(kx-\omega t)}\right)\Re\left(\left(\widetilde{U}_x\vec{x} + \widetilde{U}_y\vec{y}\right)e^{i(kx-\omega t)}\right)dt$$

And

$$\vec{j} = \frac{\rho g\omega\eta^2}{4k}\Re\left(\left(1 + \frac{H^*(\theta)}{\sqrt{kr}}e^{-i\phi(\theta)}\right)\widetilde{U}_x\vec{x} + \left(1 + \frac{H^*(\theta)}{\sqrt{kr}}e^{-i\phi(\theta)}\right)\widetilde{U}_y\vec{y}\right)$$

Expanding with the non-dimensional velocities, maintaining elements with real components to the order of $1/kr$ or greater.

$$\left(1 + \frac{H^*(\theta)}{\sqrt{kr}}e^{-i\phi(\theta)}\right)\widetilde{U}_x = 1 + \frac{1}{\sqrt{kr}}\left(H^*(\theta)e^{-i\phi(\theta)} + H(\theta)\cos\theta\, e^{i\phi(\theta)}\right) + \frac{1}{kr}H^*(\theta)\,H(\theta)\cos\theta$$

$$\left(1+\frac{H^*(\theta)}{\sqrt{kr}}e^{-i\phi(\theta)}\right)\widetilde{U}_y=\frac{1}{\sqrt{kr}}H(\theta)\sin\theta\, e^{i\phi(\theta)}+\frac{1}{kr}H^*(\theta)\,H(\theta)\sin\theta$$

So that the average energy flux can be re-written as

$$\vec{J}=P_i\cdot\Re\left(\left(1+\frac{1}{\sqrt{kr}}H^*(\theta)e^{-i\phi(\theta)}\right)\vec{x}+\left(1+\frac{1}{\sqrt{kr}}H(\theta)e^{i\phi(\theta)}+\frac{1}{kr}|H(\theta)|^2\right)\vec{u}_r\right)$$

But $\phi(\theta)=kr(1-\cos\theta)$ [2], so the two components with $\phi(\theta)$ are oscillatory. The Reimann-Lebesgue Lemma can be used to show that the asymptotic value of these terms as $r\to\infty$ is zero except at locations of stationary phase. For this function the only location of stationary phase occurs at $=0°$.

Let the interaction term equal

$$\vec{J}_i=P_i\cdot\Re\left(\frac{1}{\sqrt{kr}}H^*(\theta)e^{-i\phi(\theta)}\vec{x}+\frac{1}{\sqrt{kr}}H(\theta)e^{i\phi(\theta)}\vec{u}_r\right)$$

Close to $\theta=0°$,it is possible to suppose that $\vec{u}_r\cong\vec{x}$ so that

$$\vec{J}_i=P_i\cdot\Re\left(\frac{1}{\sqrt{kr}}\left(H^*(\theta)e^{-i\phi(\theta)}+H(\theta)e^{i\phi(\theta)}\right)\vec{x}\right)$$

This can conveniently be reduced to

$$\vec{J}_i=P_i\cdot\Re\left(\frac{2}{\sqrt{kr}}H(\theta)e^{i\phi(\theta)}\vec{x}\right)$$

Following the analysis in QUB-MF-120608-01c,

$$\lim_{r\to\infty}\vec{J}_i=\lim_{r\to\infty}P_i\Re\left(\int_{-\epsilon}^{+\epsilon}\frac{2}{\sqrt{kr}}H(\theta)e^{i\phi(\theta)}\,rd\theta\right)\vec{x}$$

Where $\pm\epsilon$ are infinitesimally small values. Using a Taylor series to approximate *cosθ* close to θ = 0° this can be written as

$$\lim_{r\to\infty}\vec{J}_i=\lim_{r\to\infty}\Re\left(\frac{P_i}{k}\int_{-\epsilon}^{+\epsilon}2\sqrt{kr}H(0)e^{ikr\frac{\theta^2}{2}}\,d\theta\right)\vec{x}$$

We now use a new integration variable, which has $\pm\infty$ as integration limits[3]

$$\alpha=\sqrt{kr}\theta$$

So that

$$\lim_{r\to\infty}\vec{J}_i=\lim_{r\to\infty}\Re\left(\frac{P_i}{k}\int_{-\infty}^{+\infty}2H(0)e^{i\frac{\alpha^2}{2}}\,d\alpha\right)\vec{x}$$

Applying known solutions

$$\lim_{r\to\infty}\vec{J}_i=\frac{2\sqrt{2\pi}P_i}{k}\Re\left(H(0)e^{i\pi/4}\right)\vec{x}$$

[22] The $\varphi(\theta)$ is included in the definition of the Kochin function

[3] This essentially follows the procedure used by Falnes in his book

Thus as $r \to \infty$ the average energy flux tends to

$$\lim_{r \to \infty} \vec{J}_i = P_i \left(\left(1 + \frac{2\sqrt{2\pi}}{k} \Re\left(H(0) e^{i\pi/4} \right) \right) \vec{x} + \left(\frac{1}{kr} |H(\theta)|^2 \right) \vec{u}_r \right)$$

As previously these three terms represent the incident wave, the reduction in the incident wave due to interactions with the wave energy converter and the waves radiated by the wave energy converter. Therefore, in the far-field approximation, the change in energy flux due to the presence of a WEC can be represented by the sum of a power absorption term and a power radiation term.